Toward a low-jitter 10 GHz pulsed source with an optical frequency comb generator

Shijun Xiao*, Leo Hollberg, Nathan R. Newbury and Scott A. Diddams

National Institute of Standards and Technology, 325 Broadway, Boulder, CO 80305
**Corresponding author: sxiao@boulder.nist.gov*

We demonstrate low residual timing jitter of 10 GHz pulses from a 1.55 μm optical frequency comb generator based on a doubly-resonant electro-optic modulator. The pulse timing jitter is analyzed, and we illustrate that the pump laser's linewidth plays a dominant role in the timing jitter. For Fourier frequencies from 1 Hz to 10 MHz, integrated residual timing jitter at 10 GHz was reduced from ~ 94 fs to ~ 8 fs when the pump laser's linewidth was reduced from ~ 10 MHz to ~ 1 kHz. An electronic servo was used to stabilize the operation point of the comb generator. With the servo, the integrated residual timing jitter was further reduced to ~ 6 fs, and the corresponding residual phase noise power density is -105 dBc/Hz at 1 Hz frequency offset from the 10 GHz pulse carrier.

OCIS codes: (120.3930) Metrology instrumentation; (120.3940) Metrology; (320.5550) Pulses; (320.5390) Picosecond phenomena.

References and Links

1. E. I. Gordon and J. D. Rigden, Bell Syst. Tech. J. **42**, 155 (1963).
2. T. Kobayashi and Y. Matsuo, "Single-Frequency Oscillation using two coupled cavities incorporating a Fabry-Pérot Electro-Optics Modulator," Appl. Phys. Lett. **16**, 217-218 (1970).
3. T. Kobayashi, T. Sueta, Y. Cho, and Y. Matsuo, "High-repetition rate optical pulse generator using a Fabry-Perot electro-optical modulator," Appl. Phys. Lett. **21**, 341-343 (1972).
4. M. Kourogi, K. Nakagawa, and M. Ohtsu, "Wide-span optical frequency comb generator for accurate optical frequency difference measurement," IEEE J. Quantum Electron. **29**, 2693-2701 (1993).
5. M. Kourogi, B. Widiyatomoko, Y. Takeuchi, and M. Ohtsu," Limit of optical-frequency comb generation due to material dispersion," IEEE J. Quantum Electron. **31**, 2120-2126 (1995).
6. K. Imai, M. Kourogi and M. Ohtsu, "30-THz span optical frequency comb generation by self-phase modulation in an optical fiber," IEEE J. Quantum Electron. **34**, 54-60 (1998).
7. T. Saitoh, S. Mattori, S. Kinugawa, K. Miyagi, A. Taniguchi, M. Kourogi and M. Ohtsu, "Modulation characteristic of waveguide-type optical frequency comb generator," IEEE J. Lightwave Technol. **16**, 824-832 (1998).
8. B. Widiyatmoko, K. Imai, M. Kourogi, and M. Ohtsu, "Second-harmonic generation of an optical frequency comb at 1.55 mm with periodically poled lithium niobate," Opt. Lett. **24**, 315-317 (1999).
9. Y. Bitou, T. R. Schibli, and K. Minoshima, "Accurate wide-range displacement measurement using tunable diode laser and optical frequency comb generator," Opt. Express **14**, 644-654 (2006).
10. http://www.optocomb.com/eng/products.html Mention of specific trade names is for technical information only, and does not constitute an endorsement by NIST.
11. G. M. Macfarlane, A. S. Bell, E. Riis, and A. I. Ferguson, "Optical comb generator as an efficient short-pulse source," Opt. Lett. **21**, 534-536 (1996).
12. R. P. Kovaich, U. Sterr, and H. R. Telle, "Short-pulse properties of optical frequency comb generators," Appl. Opt. Lett. **39**, 4372-4376 (2000).
13. M. Kato, K. Fujiura, and T. Kurihara, "Generation of a superstable Lorentzian pulse train with a high repetition frequency based on a Fabry-Pérot resonator integrated with an electro-optic phase modulator," Appl. Opt. Lett. **44**, 1263-1269 (2005).
14. Z. Jiang, D. Leaird, C. B. Huang, H. Miao, M. Kourogi, K. Imai, and A. M. Weiner, "Spectral line-by-line pulse shaping on an optical frequency comb generator," IEEE J. Quantum Electron. **43**, 1163-1174 (2007).
15. J. J. McFerran, E. N. Ivanov, A. Bartels, G. Wilpers, C. W. Oates, S. A. Diddams, and L. Hollberg, "Low-noise synthesis of microwave signals from an optical source," Electron. Lett. **41**, 36-37 (2005).
16. M. Kourogi, T. Enami, and M. Ohtsu, "A coupled-cavity monolithic optical frequency comb generator," IEEE Photon. Technol. Lett. **8**, 1698-1700,(1996).

#93770 - $15.00 USD Received 12 Mar 2008; revised 16 May 2008; accepted 17 May 2008; published 27 May 2008

17. A. S. Bell, G. M. Mcfarlane, E. Riss, and A. I. Ferguson, "An efficient optical frequency comb generator," Opt. Lett. **20**, 1435-1439 (1995).
18. U. Sterr, B. Lipphardt, A. Wolf, and H. R. Telle, "A novel stabilization method for an optical frequency comb generator," IEEE Trans. Instrum. Meas. **48**, 574-577 (1999).
19. A. L. Lance, W. D. Seal, and F. Labaar, "Phase noise and AM noise measurement in the frequency domain," in *Infrared and Millimeter Waves*, (Academic Press, 1984), Vol. **11**, 239-289.
20. http://www.covega.com Mention of specific trade names is for technical information only, and does not constitute an endorsement by NIST.

1. Introduction

Proposed in the early 1960s, the Fabry-Pérot (F-P) electro-optic modulator (EOM) [1-3] is an efficient modulation device structure, consisting of a high-speed electro-optic (EO) phase modulator is placed inside a conventional F-P cavity for resonant enhanced modulation. Originating from the F-P modulator, the optical frequency comb generator (OFCG) [4] has emerged as a valuable tool for applications in metrology, e.g., optical frequency measurements and terahertz (THz) signal synthesis and wavelength references for WDM communication systems. A major effort in previous work was to achieve combs with a wide frequency span [4-9]. In this regard, a waveguide OFCG [7, 10] turns out to be a practical device with advantages of compactness for integration and small V_π for large modulation index. On the other hand, high-repetition-rate, picosecond sources with an OFCG [7, 11-13] also gained extensive attention. Detailed properties of the pulses from an OFCG were simulated with an approximate matrix approach in [12], where the authors showed quite different temporal features depending upon operating conditions of the OFCG. In [13], 40 GHz optical pulses were generated by driving the OFCG with a 20 GHz microwave signal, and the pulse width was continuously tunable (~ 2-6 ps) by adjusting the modulation index to tune the spectral bandwidth. This provides a promising high-rate pulsed source for telecommunication applications. Most recently, novel pulse shaping and telecommunication-related experiments were demonstrated with an OFCG [14], where the manipulation of the spectral phase of individual frequency comb lines produced transform-limited picosecond pulses and arbitrary waveform generation.

Our interest in the OFCG is to evaluate its performance for low-noise optical and microwave waveform generation, as well as applications in the generation and distribution of precise time and frequency signals. Recent developments in the stabilization of continuous wave (CW) lasers have provided hertz-level optical linewidths in the visible and near infrared. When combined with an ultra-low-noise 10 GHz microwave signal in the OFCG, this could lead to a unique low-noise source with sub-radian optical phase noise and timing jitter at the femtosecond level. Important for progress along these lines is a clear understanding of the factors that determine the static phase relationship between the comb elements as well as the fluctuations of both the optical and resulting microwave phase of the emitted pulse train. In this paper, we examine the sources of excess phase noise in the pulsed output of the OFCG. We illustrate that the residual phase noise (and integrated timing jitter) on the output pulse train can be suppressed significantly by seeding the OFCG with a narrow-linewidth laser source. Both experiment and analytical results of the timing jitter are presented. These results indicate that when the OFCG is seeded with a narrow-linewidth laser and driven by a low-noise microwave signal [15], it is possible to achieve low jitter pulses with the OFCG, which will be useful for applications in high-precision metrology, time and frequency distributions, optical pulse shaping and optical arbitrary waveform synthesis.

2. OFCG properties and basic theory

Figure 1 shows the schematic characteristics of the OFCG used in our experiments (OptoComb WTEC-01 [10]). The OFCG consists of a $LiNbO_3$ waveguide phase modulator in the structure of F-P cavity. For high modulation efficiency, both the optical field and the

#93770 - $15.00 USD Received 12 Mar 2008; revised 16 May 2008; accepted 17 May 2008; published 27 May 2008

microwave field are resonant in the device. The device is compatible with standard single mode fiber and a fiber-coupled CW seed laser feeds the input port. The modulator is driven by a microwave signal, which is combined with a DC offset using a bias-T. For a symmetrical comb spectrum with the largest optical bandwidth, the microwave modulation frequency should be a multiple of the F-P cavity's free spectral range (FSR). In our case, the modulation frequency is ~10 GHz, which is four times of the F-P cavity's FSR. The temperature of the F-P cavity and waveguide is stabilized. By adjusting the temperature set point, the resonator mode spacing can be finely tuned around 10 GHz, with a tuning slope of ~ 0.02 MHz/deg in temperature range of 10-60 ^{o}C. As indicated in Fig. 1, the comb power spectrum has an approximate double-sided exponentially-decaying shape.

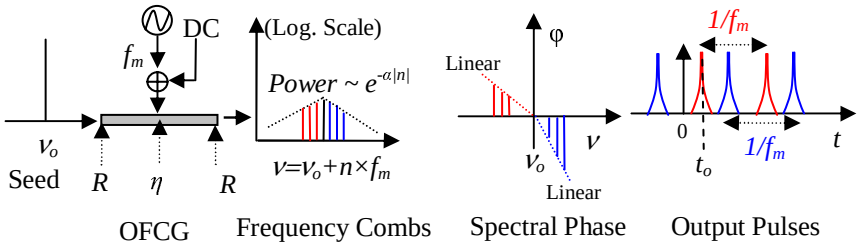

Fig. 1. Schematic principle of the OFCG: ν_o is the optical CW seed frequency, f_m is the microwave modulation frequency, R is the power reflectivity of the coatings on the two sides of the waveguide, η describes the propagation loss in the waveguide; i.e., $10 \times \log_{10}(\eta)$ is the propagation loss through the OFCG waveguide between two coatings. The time $t = 0$ in output pulse trains is referred to a sinusoidal modulation $\sin(\omega_m t)$.

For typical modulation index values ($\beta < \pi$), the two sides of the spectrum (above and below the seed frequency (ν_o) have linear spectral phases with different slopes. Since the linear spectral phase causes a constant time delay for each pulse train ($\tau = -d\varphi/d\omega$), the OFCG output is actually composed of two interleaved pulse trains with a relative time delay determined by the phase slope difference. Previous work [3, 7, 11-14] reports that the OFCG can generate two interleaved pulse trains with a relative time delay of half the modulation period (π/ω_m), which appear as a single pulse train with a repetition rate twice the modulation frequency ($\omega_m/2\pi$), and the corresponding spectral phase distribution is [0, 0, 0…] for the lower sideband and [0, π, 0, π…] or [0, π, 2π, 3π, 4π…] for the upper sideband, respectively. However, that is just a special case. More generally, the phases of the upper and lower sets of sidebands vary as the OFCG condition is changed, and the two interleaved pulse trains can have a relative time delay varying between zero to half the modulation period $T = 2\pi/\omega_m$.

Although there have been various theoretical results with the OFCG [3, 7, 11-13], here for completeness, we summarize the important time-frequency properties of the OFCG. Based on the previous theories, we present a series of key equations that compactly describe the properties of the OFCG.

When the modulation frequency is close to a multiple of the free spectral range of the OFCG cavity, the field transmission through the cavity (shown in Fig. 1) is a modified F-P formula [1-3, 7] ,

$$\frac{E_t}{E_i}(x,t,\beta) \approx \sqrt{\eta}\,\frac{1-R}{1-R\eta\exp\left[-i2\pi x - i\beta\sin(2\pi f_m t)\right]}, \qquad (1)$$

where η is the single-pass power transmission efficiency in the F-P waveguide, R is the power reflection of the F-P waveguide coating, $\beta = (V/V_\pi)\pi$ is the modulation index, and $x = \delta\nu/\mathrm{FSR} + \Phi/(2\pi)$ is the generalized detuning parameter representing the OFCG operation

#93770 - $15.00 USD Received 12 Mar 2008; revised 16 May 2008; accepted 17 May 2008; published 27 May 2008

point, where $\delta\nu = (\nu_o - \nu_{cavity})$ is the relative frequency detuning between the seed laser and the cavity resonance, and Φ is an empirically determined rf-power induced round-trip phase shift. The field transmission is a periodic function of the generalized detuning parameter x (the period = 1). For convenience, $|x| < ½$ is assumed in the following discussion. In Eq. (1), it should be mentioned that we ignore the phase delay for the first pass through the waveguide and the dispersion (both material and geometric). The finesse of the lossy F-P cavity is expressed by $F = \pi R\eta/(1-R\eta)$. One effect of the dispersion is to limit the optical bandwidth of the resulting frequency comb [5].

From Eq. (1), it can be noticed that the transmitted field is pulsed in the time domain, peaking when the phase term in the denominator is zero. For the high-finesse resonance response, each pulse's duration is much shorter than the modulation period. Based on this analysis, for time intervals around each pulse's peak, the first-order approximation of Eq. (1) is expressed by

$$\frac{E_t}{E_i}(\delta t) \approx \sqrt{\eta}\,\frac{1-R}{(1-R\eta)+iR\eta\beta\omega_m\cos(\omega_m t_o)\delta t}, \tag{2}$$

where $\delta t = t - t_o$ and $|\delta t| \ll 1/f_m$, and t_o (marked in Fig. 1) is the pulse peak timing position, which satisfies

$$2\pi x + \beta\sin(\omega_m t_o) = 0, \tag{3}$$

valid for $|x| < \beta/2\pi$, or

$$t_o = -\frac{1}{\omega_m}\sin^{-1}\left(\frac{2\pi x}{\beta}\right). \tag{4}$$

This equation has two solutions, t_L and t_U related by $t_L + t_U = T/2$, corresponding to the two pulse trains (blue and red) illustrated in Fig. 1. For each pulse train, Eq. (2) predicts pulses that are Lorentzian in time, with a pulse width at half maximum intensity of

$$\tau_{FWHM} = \frac{1}{F\beta f_m\sqrt{1-\left(\frac{2\pi x}{\beta}\right)^2}}. \tag{5}$$

which is a minimum when x is zero. The pulse peak power transmission at $\delta t = 0$ doesn't vary with the OFCG operation point, but is determined by the F-P cavity parameters. As shown in Fig. 1 and discussed in Ref. [4], the corresponding spectra for the two pulse trains are single-sided exponentials (the Fourier transform of a Lorentzian) distributed symmetrically on the lower and upper sides of the seed laser frequency with a characteristic 1/e spectral width $(2\pi\tau_{FWHM.})^{-1}$. The maximum spectral bandwidth is achieved at minimum pulse width or $x = 0$, according to Eq. (5).

We are particularly interested in the timing jitter. From Eq. (4), the root-mean-square (RMS) timing jitter is

$$\tau_{jitter} = \frac{\sigma_x}{\beta f_m}\frac{1}{\sqrt{1-\left(\frac{2\pi x}{\beta}\right)^2}}, \tag{6}$$

where σ_x represents the standard deviation of the fluctuation of x. The timing jitter gets smaller when β is larger and at $x = 0$. The standard deviation of the fluctuation of x is determined by the seed laser frequency jitter, $\Delta\nu_{seed}$, the frequency jitter of the F-P cavity resonance, $\Delta\nu_{cavity,}$ and the round-trip phase noise, $\Delta\Phi$. If these noise sources are uncorrelated, σ_x can be written as

#93770 - $15.00 USD Received 12 Mar 2008; revised 16 May 2008; accepted 17 May 2008; published 27 May 2008

$$\sigma_x = \sqrt{\left(\frac{\Delta\upsilon_{seed}}{FSR}\right)^2 + \left(\frac{\Delta\upsilon_{cavity}}{FSR}\right)^2 + \left(\frac{\Delta\Phi}{2\pi}\right)^2}\,, \tag{7}$$

Later we find that the round-trip phase noise also depends on the rf power so that $\Delta\Phi = |d\Phi/d\beta|\times\Delta\beta$, where $\Delta\beta$ is the standard deviation of the modulation index fluctuation. From Eq. (7), narrow-linewidth seed lasers, stable optical cavities and low-noise modulation signals are necessary to achieve low timing jitter.

Finally, one more useful result is the time-averaged power transmission, $P_{avg,}$. From Eq. (2), we find

$$\frac{P_{avg}}{P_{seed}} = \frac{1}{T}\int_0^T \left|\frac{E_t}{E_i}(\delta\nu, t, \phi)\right|^2 dt = \frac{2}{T}\int_0^T \eta\,\frac{(1-R)^2}{(1-R\eta)^2 + \left[R\eta\beta\omega_m\cos(\omega_m t_o)\right]^2 t^2}dt\,, \tag{8}$$

where P_{seed} is the CW seed power. The factor of two before the integral is due to the two identical pulses in each modulation period. This integral yields

$$\frac{P_{avg}}{P_{seed}} = \frac{(1-R)^2}{\pi R(1-R\eta)\beta\times\sqrt{1-\left(\frac{2\pi x}{\beta}\right)^2}}\times\arctan\left[\frac{2\pi R\eta\beta}{1-R\eta}\sqrt{1-\left(\frac{2\pi x}{\beta}\right)^2}\right], \tag{9}$$

again valid only for $|x| \le \beta/2\pi$. For analytical cases, instead of Eq. (1), Eq. (2) is used directly. According to Eq. (9), the time-averaged power transmission varies with the OFCG operation point. The transmission is minimum at $x = 0$. The transmission increases as $|x|$ increases from 0 to $\beta/2\pi$, and it becomes maximum when $|x| \rightarrow \beta/2\pi$. It is therefore a useful means to identify the detuning parameter and value of β experimentally, as is done in the next section.

To briefly conclude this section, the response of the OFCG is determined by its operation point that is represented by the parameter x. The most interesting case is $x = 0$, where the OFCG yields the maximum bandwidth (the narrowest pulse) as well as the lowest residual timing jitter for a fixed modulation index. However, the minimum power transmission also occurs at $x = 0$. Another useful result is the pulse-rate doubling effect for the OFCG at $x = 0$.

3. Experiments of basic OFCG properties

Our OFCG was driven at 10 GHz with a cavity reflectivity of R = 0.97 (manufacturer's specification) and transmission efficiency of η = 0.9763 (our calibration), corresponding to a round-trip loss of 0.208 dB. The effective finesse of the optical F-P cavity is 60. In our device, the maximum power transmission is only 30 % (about 5.2 dB loss), which is caused by the waveguide propagation loss (η<1). This loss does not include the fiber-to-waveguide coupling loss. Figure 2 shows the calculated time-averaged power transmission versus the normalized relative detuning $\delta\upsilon$/FSR for different modulation indices β and our parameters. (These calculations used Eq. (1) rather than the approximation (2)). As discussed in Section 2, for $\beta < \pi$, each resonance peak symmetrically splits into double peaks, and the power is maximum at detunings approximately equal to $\beta/2\pi$. On other hand, the maximum comb bandwidth occurs at zero detuning, but, the average power loss is also the largest at this point. For modulation index greater than π but less than 2π, the curves repeat but with the center shifted to the position with $\delta\nu$/FSR = 1/2.

#93770 - $15.00 USD Received 12 Mar 2008; revised 16 May 2008; accepted 17 May 2008; published 27 May 2008

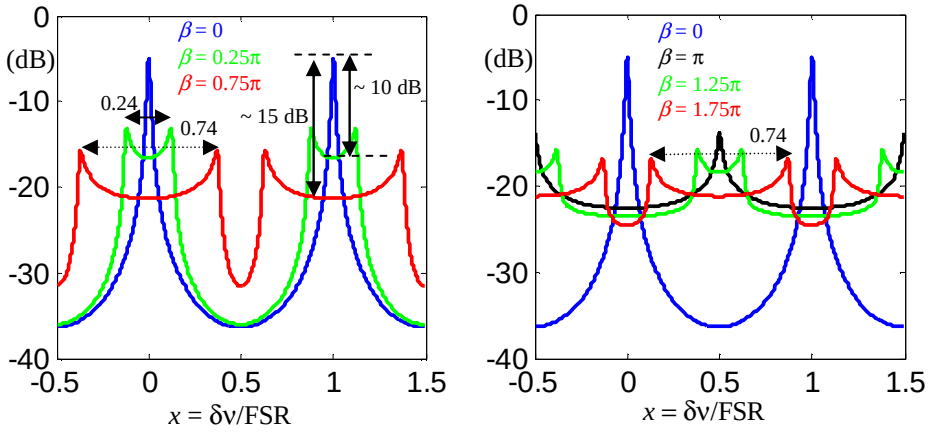

Fig. 2. Calculated time-averaged power transmission versus the normalized frequency detuning. $\Phi = 0$ is assumed. Curves for several different values of β are shown.

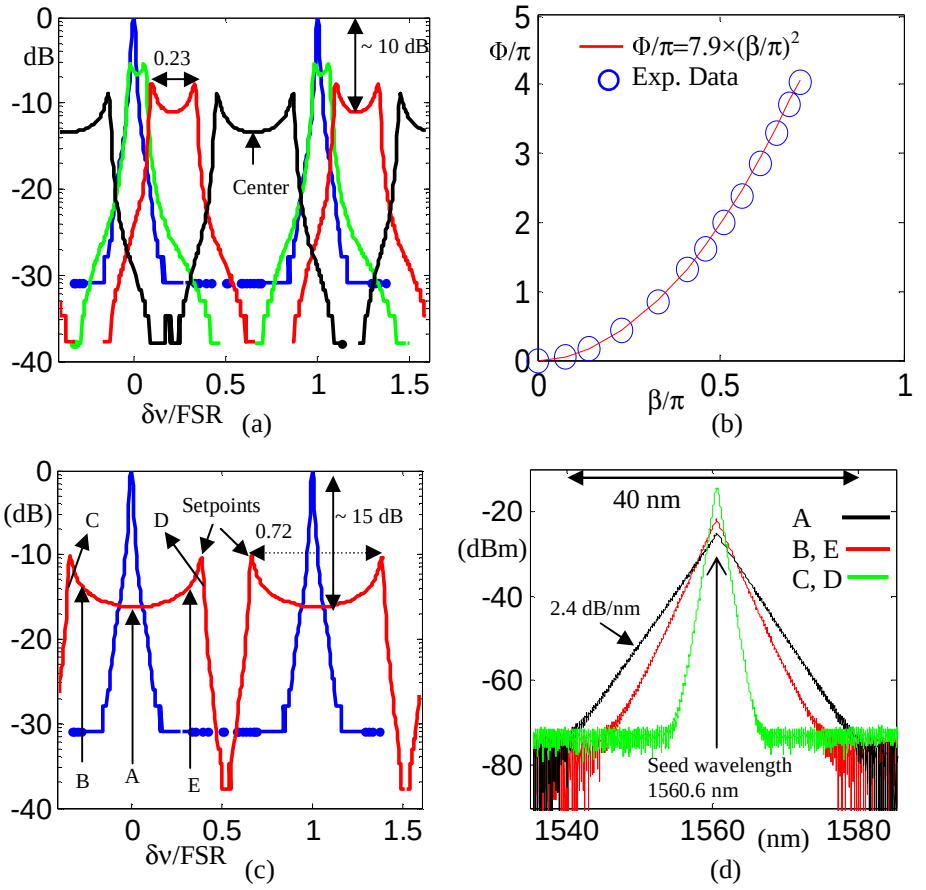

Fig. 3. (a). Experimental time-averaged power transmission as a function of the normalized detuning between the cavity and the pump. The blue, green, red and black curves are for different drive RF powers of around 0, 5, 14 and 19 dBm, respectively. (b) Experimental round-trip static phase shift induced by increasing the microwave power applied to the OFCG, presumably due to heating. (c) Experimental time-averaged power transmission vs. frequency detuning for $\beta \approx 0.72\ \pi$ (red curve); the reference with $\beta = 0$ (blue) is also plotted. A, B, C, D and E represent five different frequency detunings. (d) measured spectra (1 nm resolution) at the six operation points.

#93770 - $15.00 USD Received 12 Mar 2008; revised 16 May 2008; accepted 17 May 2008; published 27 May 2008

Figure 3(a) plots the experimentally measured time-averaged power transmission with different modulation indices. By using a sweeping bias voltage to tune the relative frequency detuning parameter $\delta\nu$, the time-averaged optical power was detected by a low-speed (50 MHz bandwidth) photodiode. In general, the agreement with Fig. 2 is excellent, except for the low transmission in the wings. Figure 3(b) plots the measured data (blue circles) of $\Phi(\beta)$ vs. β, where β was calculated from the peak splitting. We found that a quadratic curve was sufficient to fit the data, and this means that the phase shift is proportional to the RF driving power. The phase shift may be attributed to heating of the waveguide that results from increasing RF power. The red curve of Fig. 3(c) plots the experimental time-integrated transmission of the OFCG with a largest modulation index ($\beta \approx 0.72\ \pi$), and the blue curve is the reference with zero modulation. For $\beta \approx 0.72\pi$, we have $\Phi \approx 4\pi$, and it is equivalent to set $\Phi = 0$ for simplicity. Thus, we have $x = \delta\nu/\mathrm{FSR}$. The output spectra at different operation points (A, B, C, D and E) were observed by tuning the bias.

Figure 3(d) plots the measured optical power spectrum at different operation points at 1 nm spectral resolution. For the operation point A ($x = 0$), the generated frequency comb spans almost 40 nm (5 THz) before reaching the measurement noise floor. For optical spectrum on each side of the seed wavelength, the power decays linearly in the log scale, and the slope is 2.44 dB/nm, or 0.195 dB per comb line. At the operation point A, $\beta = 0.72\pi$ and F = 60, giving a theoretical power decaying coefficient of 0.2 dB per comb, which agrees well with the experiment. For operation points away from A ($|x| \rightarrow \beta/2\pi$), the sideband power decays faster, and the bandwidth becomes narrower. Our identification of these OFCG operation conditions related to power transmission is useful to understand the timing properties (pulse characteristics and timing jitter) discussed in the following sections. As discussed earlier, the operation point A ($x = 0$) will yield the narrowest, most stable output pulse trains.

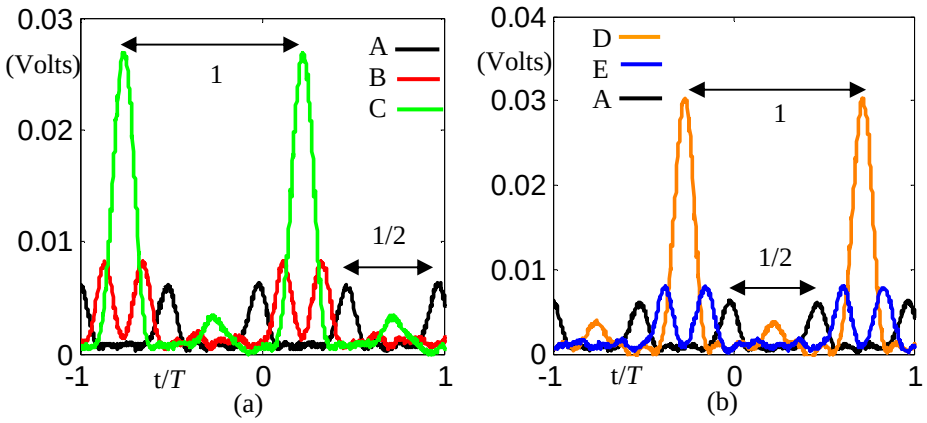

Fig. 4. (a)-(b) Measured output pulses for different OFCG operation points.

Figures 4(a)-4(b) show output pulses at different operation points, detected by a high-speed photodiode (~ 9 ps pulse width at half maximum for its impulse response) and then measured by a fast sampling scope. The electronic resolution can't resolve the short pulse here as well as the pulse peak power. The modulation index is 0.72π. Our focus here is to see the timing delay related to the linear spectral phase, and the electronic measurement is sufficient for this purpose. The horizontal time axis is normalized to the modulation period $T = 1/f_m \approx 100$ ps. For frequency detuning satisfying $x = 0$, e.g., operation point A, the output is a superposition of two 10 GHz pulse trains that form a 20 GHz pulse train. When

#93770 - $15.00 USD Received 12 Mar 2008; revised 16 May 2008; accepted 17 May 2008; published 27 May 2008

the operation point changes from A to B, the relative delay of two 10 GHz pulse trains is smaller than half the modulation period, and the pulse trains tend to overlap each other in the time domain. When the operation point switches from B to C and across the setpoint (the maximum transmission) marked in Fig. 3(c), the two 10 GHz pulse trains are broadened and merge into a single 10 GHz pulse train, which is the same situation for D. However, there is still a weak 10 GHz pulse train remaining, and this indicates more complex pulse properties beyond what is based on Eq. (1). Roughly speaking, output pulses at operation points C and D have the same relative delay (half the modulation period) but different delay signs when referred to the pulses generated at A. We can have similar results when comparing output pulses at operation points B and E. We also calculate these output pulses from Eq. (1) by setting x = 0, -0.292, -0.373, 0.361, and 0.290 (for A, B, C, D and E) to match with the bias detuning in experiments. Generally speaking, the calculation agrees well with the electronic measurement on the pulse timing position.

4. Measurements of timing jitter

Short-pulse sources with low jitter and high repetition rate are important in a variety of scientific and technological fields [15]. However, there have been few reports on timing jitter and phase-noise characteristics of the pulses generated by a modulator-based OFCG. In [12], a rough estimation of the residual timing jitter due to the frequency fluctuation of seed lasers was given. Although the frequency comb spacing is precisely determined by the modulation frequency, large residual timing jitter can still exist due to the fluctuation of the phase of each comb line. As analyzed in Section II, the pulse timing position fluctuates due to random variations of the seed laser's frequency, the cavity resonance frequency and the modulation power. It is desirable to lock the OFCG cavity to a narrow-linewidth optical seed and use low-jitter modulation for applications requiring the highest stable short-pulse sources. While there has been work on stabilizing the OFCG [5, 18], the effect on timing jitter and corresponding microwave phase-noise was not reported. In this section, we illustrate that the residual phase noise (and integrated timing jitter) can be suppressed significantly by seeding the OFCG with a narrow-linewidth fiber laser rather than a semiconductor DFB laser. With a servo to stabilize the OFCG operation point, the timing jitter and the phase noise can be further reduced.

Section II presented a theoretical expression for the timing jitter (Eq. (6)) and it is interesting to consider the specific parameters relevant to our system. In order to focus on the frequency noise of the seed laser and the cavity, we neglect the fluctuation of the modulation index; i.e., $\Delta\beta = 0$. For our system, FSR = 2.5 GHz, $\beta = 0.72\pi$ and f_m = 10 GHz. The unlocked F-P cavity's integrated frequency jitter was measured to be 25 kHz from 1Hz to 10 MHz. From Eq. (6), at x = 0, the timing jitter caused by the cavity's frequency jitter is only about 0.4 fs. In contrast, for our DFB seed laser, we measured $\Delta\nu_{seed} \approx$ 10 MHz, which leads to an estimated timing jitter of about 177 fs at x = 0. For timing jitter < ~ 1 fs at f_m = 10 GHz, narrow-linewidth (< ~ 50 kHz) seed laser is required. We note that for stable long-term operation, the OFCG operation point should also be locked with a servo system.

Figure 5 shows our experimental setup that employs a hybrid optical/microwave phase bridge to measure the residual phase noise of the pulses from the OFCG [19]. The lower arm of the bridge incorporates a Mach-Zehnder modulator (MZM) [20] which allows us to match the delay of the upper arm without the impractical introduction of long microwave cables. The conversion from microwave to optical (MZM), the 40 meter fiber link, and conversion back to microwave (PD2) was independently verified to have phase noise below that measured for the OFCG. The linewidth of the laser source input to the MZM doesn't contribute appreciably to the phase noise of the delay matching arm. The delay matching error was $\leq$ 5 ns. Thus, for the Fourier frequencies range 1Hz to 10 MHz, the microwave source's phase noise did not degrade the measured residual phase noise spectrum. In order

#93770 - $15.00 USD Received 12 Mar 2008; revised 16 May 2008; accepted 17 May 2008; published 27 May 2008

to obtain a single pulse train at f_m from the OFCG, we select one half of the comb spectrum (it is equivalent to select either the lower or upper half of the optical spectrum).

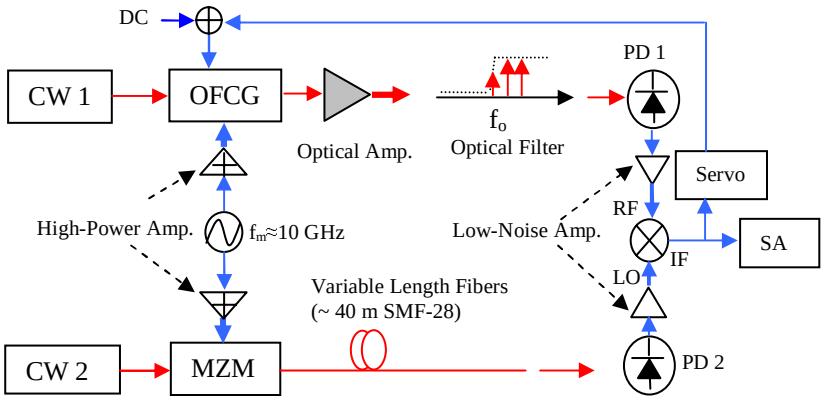

Fig. 5. Experimental setup to measure the residual phase noise of pulses from OFCG. The optical filter is a blocking filter that selects one half comb spectrum corresponding to one f_m pulse train. The blocking filter is in the well known reflective Fourier-transform pulse-shaper geometry based on a diffraction grating, and a hard aperture was used to block half the optical spectrum. The variable length fibers were used to match the relative delay. SA: spectrum analyzer. PD is an InGaAs photodiode. MZM: Mach-Zehnder Modulator (Mach-10002 [20]).

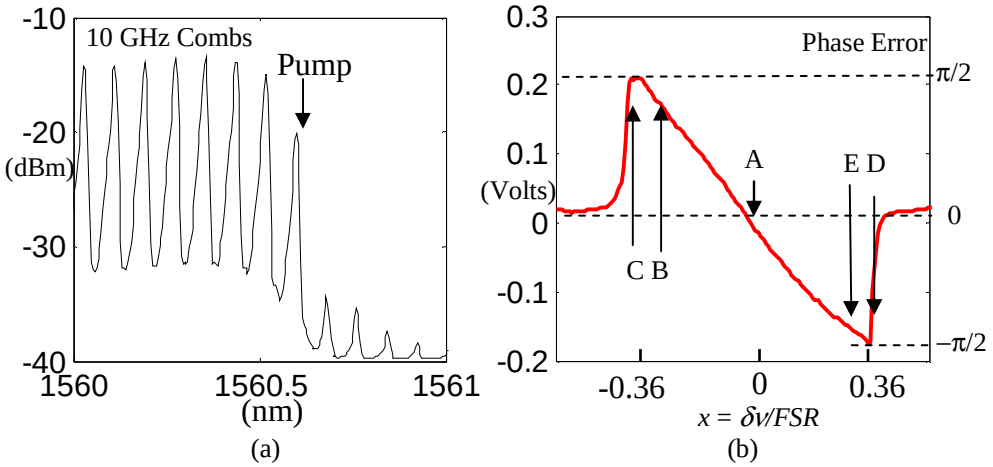

Fig. 6. (a). Comb spectrum after the optical filter when the higher-frequency sideband was selected. (b). Measured phase error signal at the mixer IF port as a function of the operating point.

Figure 6(a) illustrates the filtered comb spectrum after the optical filter, where the high-frequency (n≥0) side of the spectrum was selected, corresponding to a 10 GHz pulse train. Before the optical filtering, the OFCG output (power ~ -10 dBm) was amplified by an erbium-doped fiber amplifier (EDFA). As the phase difference is proportional to the timing delay difference between the two arms of the bridge, the error signal at the mixer intermediate frequency (IF) is sensitive to the OFCG operation point. Figure 6(b) shows the phase error signal at different OFCG operation points, measured by sweeping the DC bias. The error signal from the mixer was set to zero volts DC at the operation point A, where the OFCG was stabilized with a servo. The servo is an integrator that efficiently

#93770 - $15.00 USD Received 12 Mar 2008; revised 16 May 2008; accepted 17 May 2008; published 27 May 2008

suppresses low-frequency noises. Fluctuations in the mixer output voltage correspond to the relative phase noise and were measured with an FFT spectrum analyzer.

Figure 7 plots measured residual phase noise within the frequency range of 1 Hz to 10 MHz. The measurement was carried out at the operation point of $x = 0$, where the theoretical timing jitter is minimum when compared to other choices of x. We tried two different optical seed lasers, a DFB laser (wavelength ~ 1542 nm) and a narrow-linewidth fiber laser (wavelength ~ 1560 nm). The measured linewidth of the DFB laser is on the order of 10 MHz. The manufacture specification of the fiber laser's linewidth is less than 400 Hz. The fiber laser source was sent to our lab through 200 meter optical fiber (SMF-28); this transport would likely increase the linewidth to several kHz based on previous measurements. As predicted, Fig. 7(a) shows a significant difference between the phase noises of the OFCG with these two different seed laser sources. The system noise floor was measured by removing the OFCG from the bridge and directly connecting (through RF power attenuators) the high-power μ-wave amplifier that drove the OFCG to the RF port of the μ-wave mixer. The noise floor is limited mainly by the two high-power (27-30 dBm) μ-wave amplifiers. Other noise sources include the MZM, photodiode (1/*f* and shot-noise), low-noise μ-wave amplifiers and the microwave mixer, which provide lower noise floors than that from the high-power μ-wave amplifiers. In Fig. 7 (b), at frequencies less than 10 Hz, the noise of the servoed system falls below that of the measurement floor because 1/f noise is suppressed by the servo. This 1/f noise was not suppressed in the open-loop measurement of the noise floor. The large difference in the phase noise with the different CW pumps is clearly demonstrated in these experiments. Better attention to ground loops and shielding of the system should remove the strong spikes on the phase noise PSD corresponding to 60 Hz harmonics. Other spikes at higher frequencies are from active components (OFCG, optical amplifiers), and pick-up from surrounding electronics and the seed lasers.

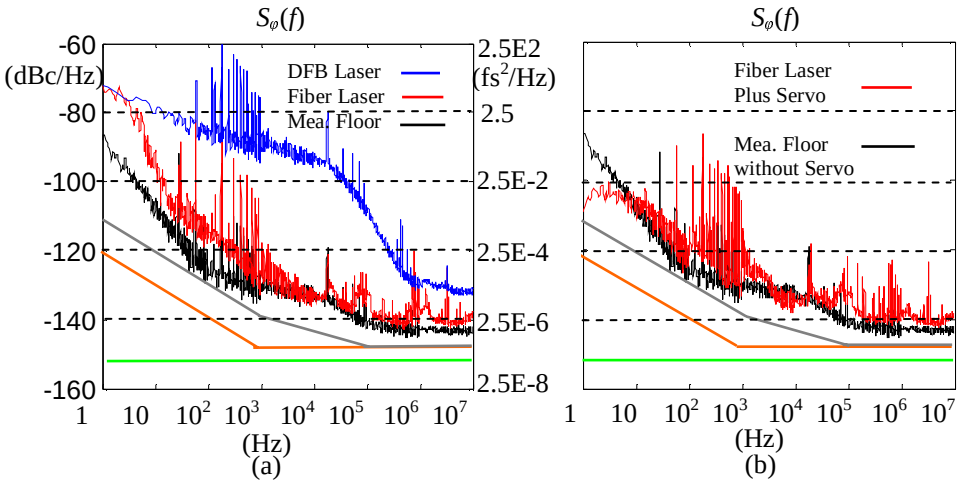

Fig. 7. (a). Measured residual phase-noise PSD $S_\varphi(f)$ at 10GHz with two different pump lasers. (b) Measured phase-noise PSD with the narrow-linewidth pump laser as well as the servo control system. The gray, orange and green lines indicate mixer noise, spectrum analyzer noise and photodiode shot-noise level, respectively, in our measurement system. The MZM did not add appreciable noise above the mixer noise's floor.

The relation between the RMS timing jitter and the phase noise is expressed by

$$\tau_{rms} = \frac{1}{2\pi f_m}\sqrt{\int_{f=0}^{f=f_m/2} S_\varphi(f)\,df}\ , \qquad (10)$$

#93770 - $15.00 USD Received 12 Mar 2008; revised 16 May 2008; accepted 17 May 2008; published 27 May 2008

where $S_\varphi(f) = 2L(f)$ and $L(f)$ represents the single sideband phase-noise power spectral density (PSD). In practice, we measure the total noise PSD for a certain bandwidth, e.g., 1 Hz to 10 MHz, provided by the FFT spectrum analyzer. From Fig. 7(a), the noise PSD decays quickly and reaches the system noise floor at higher frequencies (~1 MHz). We have not measured the phase noise PSD for the full bandwidth up to $f_m/2 \approx 5$ GHz, although we do not expect any rise in the noise floor above that at 10 MHz. For the measurement floor (black), the 10 GHz integrated phase noise from 1 Hz to 10 MHz is 5.9×10^{-8} rad^2, which corresponds to a timing jitter of 3.9 fs, which is the lowest bound of measurable timing jitter in our current system without servo. Table 1 lists the residual integrated phase noise power (rad^2) and the corresponding timing jitter (fs) for two different seed lasers with different linewidth. For each seed laser, two results (with servo and without servo) are presented. Figure 7(b) shows an example of measured phase noise with the fiber laser seed plus servo control. As our measurements were limited to the frequency range of 1 Hz to 10 MHz, for the DFB laser, the obtained timing jitter (94 fs) should be smaller than the theoretical prediction (177 fs at $x = 0$) in Section IV. We believe that the phase noise and the timing jitter could be further reduced with low-noise optical and microwave amplifiers, and high-speed low-noise servo control. Ultimately, an OFCG seeded with a narrow-linewidth frequency stabilized laser and driven by low-noise microwave signals [15] should provide a stable and low-jitter optical pulse train and frequency comb.

Table 1. Experimental residual phase noise and residual timing jitter for different seed lasers.

	DFB (Linewidth ~ 10 MHz)	Fiber Laser (Linewidth ~ 10 KHz)
Without Servo	3.5×10^{-5} rad^2 94 fs	2.8×10^{-7} rad^2 8.4 fs
With Servo	1.4×10^{-6} rad^2 20 fs	1.6×10^{-7} rad^2 6.4 fs

5. Conclusion

Timing jitter characteristics of an OFCG have been presented with theory and experiments. Although this study focused on an OFCG that generates 10 GHz-spaced frequency combs at 1.55 μm, our results can apply to OFCG at other wavelengths and with different modulation frequencies. Two sides of the optical spectrum from the OFCG correspond to two pulse trains with a timing delay varying between zero and half the modulation period. For each pulse train, the delay is sensitive to random drifts of the OFCG operation point, and the noise of the operation point results in excess pulse timing jitter. Analytical results of the timing jitter are derived, and we show that the residual jitter originates from noise of the seed laser frequency, the cavity resonance and the modulation source. Experimentally, for the first time, we have demonstrated residual timing jitter of less than 10 fs (measured bandwidth 1 Hz-10 MHz) for 10 GHz OFCG pulses, which indicates a relative phase uncertainty < 7×10^{-4} radians between two adjacent 10 GHz comb lines. Our results demonstrate that the OFCG is a promising option for a low-timing-jitter, high-repetition-rate short-pulse source.

Acknowledgments

We thank M. Kourogi, K. Imai and T. Asaeda for their assistance with the optical comb generator and Andy Weiner for valuable discussions. This work was supported by NIST and DARPA. This paper is a contribution of an agency of the US government and not subject to copyright in the US.

#93770 - $15.00 USD Received 12 Mar 2008; revised 16 May 2008; accepted 17 May 2008; published 27 May 2008